Lightweighting structures using an explicit microarchitectured material framework

Antonio Di Rienzo, Edouard Duriez, Miguel Charlotte, Joseph Morlier

▶ **To cite this version:**

Antonio Di Rienzo, Edouard Duriez, Miguel Charlotte, Joseph Morlier. Lightweighting structures using an explicit microarchitectured material framework. EDP Sciences, 2024, 25 (7), pp.7. 10.1051/meca/2024004 . hal-04512430

HAL Id: hal-04512430
https://hal.science/hal-04512430

Submitted on 20 Mar 2024

HAL is a multi-disciplinary open access archive for the deposit and dissemination of scientific research documents, whether they are published or not. The documents may come from teaching and research institutions in France or abroad, or from public or private research centers.

L'archive ouverte pluridisciplinaire **HAL**, est destinée au dépôt et à la diffusion de documents scientifiques de niveau recherche, publiés ou non, émanant des établissements d'enseignement et de recherche français ou étrangers, des laboratoires publics ou privés.

Mechanics & Industry **25**, 7 (2024)
© A. Di Rienzo et al., Published by EDP Sciences, 2024
https://doi.org/10.1051/meca/2024004

Mechanics & Industry

Available online at:
www.mechanics-industry.org

REGULAR ARTICLE

OPEN ACCESS

Lightweighting structures using an explicit microarchitectured material framework

Antonio Di Rienzo[1,2,*], Edouard Duriez[1], Miguel Charlotte[1], and Joseph Morlier[1]

[1] ICA, Université de Toulouse, ISAE-SUPAERO, MINES ALBI, UPS, INSA, CNRS, Toulouse, France
[2] Università di Pisa, DICI, Pisa, Italy

Received: 21 May 2023 / Accepted: 18 January 2024

Abstract. In this paper, a new approach to design ultralight structures is developed based on a previous work called Efficient Multiscale Topology Optimization. A parameterized (or explicit) truss-based cell is introduced to generate intrinsically well-connected microstructures and to get clear interpretable optimal multiscale structures. The method uses a pre-computed database of optimal micro-cells to be computational efficient without losing in structural performances. The parameterization allows to generate a lightweight database just storing the set of parameters, that define the optimal cells, and the cells properties, that are obtained through inverse homogenization. The method has been successfully tested on two-dimensional compliance problems. Several examples demonstrate its versatility and give quantitative results. Moreover, it allows to obtain structures compatible with additive manufacturing processes, to naturally solve concurrent multi-scale problems, as well as controlled porosity and optimal fiber orientation problems.

Keywords: Structural optimization / multi-scale design / architectured material design / additive manufacturing / homogenization

1 Introduction

1.1 Context

Topology optimization is a mathematical method to find the optimal distribution of material or structural elements within a design space, for given loads and boundary conditions with the objective to maximize the performances of the structure while respecting constraints. The first general theory of topology optimization was formulated by Prager and Rozvany [1] and lots of different methods have been developed starting from this point: the homogenization method [2], the Solid Isotropic Material with Penalization (SIMP) [3], the inverse homogenization method [4], the evolutionary structural optimization (ESO) [5], level set method (LSM) [6] and others.

The structures resulting from a topology optimization have better performances but higher geometry complexity. Therefore, due to manufacturing difficulties, in the late 1990s, the so called "mono-scale" approaches are mainly developed, optimizing the distribution of a homogeneous isotropic material (SIMP) [7,8]. However, the latest advancements in additive manufacturing (AM also known as 3D printing) led to a new interest in the design of multi-scale structures, where each macro point can be represented as a local "microscopic" structure. Therefore, the design of architectured materials or meta-materials is having a great development since materials with exceptional properties, that cannot be found in nature, can be obtained, such as maximized bulk or shear modulus [4,9,10], negative Poisson's ratio [11], negative thermal expansion [12]. The previous approaches studied periodically repeated micro-structures but in the industrial field the assemblies of optimized micro-structure, with spatially-varying properties, are of great interest since they allow to achieve structures with optimized characteristics. The issue is how to get optimized micro-structures that are compatible with their neighbours.

The design of architectured materials can be achieved by a multi-scale topology optimization (MTO), which consists in optimizing both the macro-scale and the micro-one. An exhaustive review of several methods about MTO was done by Wu et al. [13]. The MTO faces two main issues that are:

– Connecting neighbouring micro-structures without reducing too much the solution space. A bad connection (or compatibility) does not allow the load to be transferred correctly and therefore the properties of the micro-structures obtained through homogenization are not representative of how the whole structure will react.

* e-mail: a.dirienzo3@studenti.unipi.it

This is an Open Access article distributed under the terms of the Creative Commons Attribution License (https://creativecommons.org/licenses/by/4.0), which permits unrestricted use, distribution, and reproduction in any medium, provided the original work is properly cited.

– Optimizing simultaneously the two scales has a high computational cost.

Various approaches and methods in literature have been developed by considering these two issues. For instance, Wang et al. [14] presented a framework that uses a multi-scale isogeometric topology optimization to optimize the relative density of lattice materials. In that last work, four unit-cells with well-defined topologies are predefined and their properties are expressed as functions of the relative density and directly used in the optimization loop, improving the computational efficiency. A similar approach is the one of Watts et al. [15] that considered three open truss unit cells, compatible with many additive manufacturing techniques, for which accurate surrogate models of the properties as function of the relative density are obtained through homogenization. Once selected one of the three possible topologies of the unit cell, it is kept constant over the design domain with the possibility to vary its geometry through the domain within defined bounds.

To improve the connectivity between cells Zhou and Li [16] presented three methods namely connective constraint, pseudo load and unified formulation with nonlinear diffusion. In the first two methods, the unit cells are optimized individually imposing constraints to connect them with predefined common regions. In the third method, the unit cells are optimized all together and a nonlinear diffusion term is introduced in the objective function suppressing checkerboard patterns and blurred boundaries, thereby ensuring proper topological interconnections. Also Garner et al. [17] presented a method to assure connectivity between adjacent cells, optimizing simultaneously the physical properties of the individual cells as well as those of neighbouring pairs. Therefore, they ensure material connectivity and the smooth variation of the physical properties.

Xia and Breitkopf [18] proposed a finite element square nonlinear multi-scale analysis framework for concurrent design of the materials and structures. However, the computational cost is quite massive due to a large number of instant local material optimizations. Therefore, Xia and Breitkopf [19] introduced a reduced database model to approximate the material behaviour. The approximate constitutive model for locally optimized material is built off-line and the structural optimization using the precomputed constitutive model is performed on-line, improving the computational efficiency. Precomputed databases have also been proposed for parametrized lattice cells, obtaining a polynomial model to access cells in between database points [20–23].

It is also worth mentioning lately some works such like Pantz and Trabelsi [24], Allaire et al. [25], Goeffroy-Donders et al. [26], or Groen and Sigmund [27], which also combine topology optimization and periodic homogenization theory in a different way. Indeed, they rather considered some post-processing de-homogenization (or "inverse homogenization") treatments that consist in replacing an optimized homogenized design by a periodic lattice. The process involves notably as well an orientation regularization and a projection algorithm onto a specific family of parametrized micro-cells (with cubic or square symmetry). Their inverse homogenization strategies differ from the one presented hereafter and that intends to use a pre-computed database of micro-cells (defined as clusters of beams) in order to be computational efficient without losing in structural performances.

The remaining part of this paper is organized as follows. Section 2 of this article briefly describes the main contributions of the Efficient Multiscale Topology Optimization (EMTO) method and provides the objective of this work. In Section 3 a new explicit approach (Ex-EMTO) is developed by defining a parametrized truss-based unit cell, describing the micro-scale and macro-scale optimization problems and explaining the database construction with a first comparison with the original EMTO. Section 4 provides some comparison with the original EMTO and with other strategies on classical problems and shows clear interpretable structures obtained with the new approach. In Section 5, the versatility of the method is demonstrated by solving different types of problems. Finally, Section 6 concludes the paper with final remarks and with suggested future work.

2 Efficient multiscale topology optimization

We extend here previous works of the authors of EMTO for the 2D problems [28]. The EMTO consists in optimizing the micro and the macro scales separately. The micro-scale topology optimization is used to create off-line a database of micro-structures to use in the macro-scale topology optimization to obtain competitive structure reducing the computational cost. The EMTO method tries to answer to the previous issues of multi-scale approach (connectivity and computational cost) while assuring micro-structures to follow local stress or strain. The main contributions are:

– The definition of the so-called "adaptive transmission zones" in the 2D micro-structure. In order to ensure well connected micro-structure, a number of connection points is set along the border of the unit cell. Depending on these connection points, the transmission zones are defined as portions of the borders of the unit cell where the material eventually is enforced to be. In this way stresses can only be transmitted through those zones from a unit cell to the neighbour cells. The transmission zones are adaptive because depending on the conditions they can change their sizes, resulting in very low design constraint.
– The introduction of well-chosen variables to bridge the macro-scale and the micro-scale. In the simplest forms of MTO, only the density variable is used. In the EMTO, the orientation of the cell (that corresponds to a rotation of the cell with respect to the out-of-plane direction) and a variable called cubicity (that quantifies the relative importance of the two principal directions in 2D case) are added as variables too. This allows to follow better the principal stresses and to consider their relative intensity difference. Therefore, density, orientation and cubicity are called macro-variables. So, at the end of the macro-scale optimization a set of these three variables is given

(a) Micro-structures obtained for different density values: 0.25, 0.5, 0.75.

(b) Micro-structures obtained for different orientation values: 0, $\pi/12$, $\pi/6$, $\pi/4$.

(c) Micro-structures obtained for different cubicity values: 0, 0.5, 1.

Fig. 1. Influence of the 3 macro-variables on a micro-structure Boxed in green the unit cell having density 0.5, orientation $\pi/4$ and cubicity 0. In each subfigure, two of these variables are fixed, while the third varies.

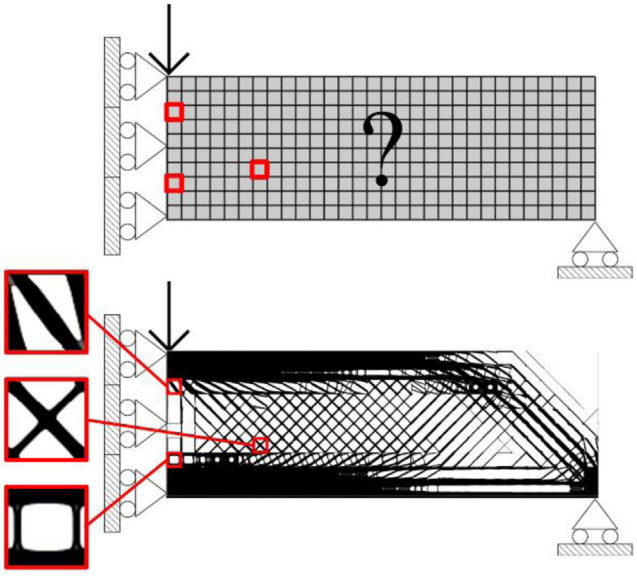

Fig. 2. Original EMTO half MBB beam solution. In red some cells are highlighted to show the apparent truss structure.

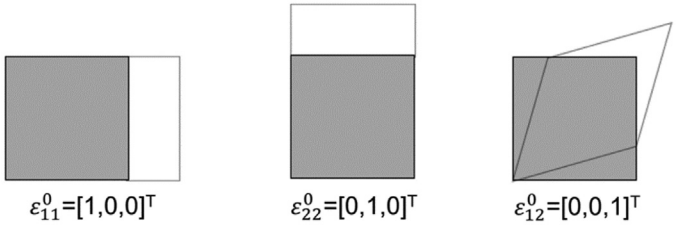

Fig. 3. The unit test strain fields imposed on a 2D unit cell.

for each macro element. Examples of how the micro-structure changes depending on the macro-variables are shown in Figure 1.

– A database containing both the structural architecture and the properties of the unit cells, to have a faster computation in the macro-scale optimization. The database is built on a regularly spaced 3-dimensional grid of the three macro variables in order to have micro-structures close to any point of the design space. This means that, for any given set of macro-variables assumed by a macro-element, during and at the end of the macro-optimization, is possible to find inside the database a micro-structure with relative properties that satisfy quite well the conditions given by the set of macro-variables.

The objective of this paper is a further validation of the original EMTO method and also a demonstration of its flexibility. Original EMTO shows that the full-scale structure tends to be truss-like as shown in Figure 2 with lot of internal forces redistribution. Therefore, a new explicit approach, called Ex- EMTO, to build the database of the unit cells (parametrized with a manufacturable assembly of beams) is developed and the existing EMTO macro-codes are adapted to the new obtained database, with the aim at obtaining clear interpretable micro-structures too. The framework is open-source and available on GitHub for reproducible research purpose (https://github.com/mid2SUPAERO/Ex-EMTO).

Following the original EMTO, the micro-scale optimization gives as results optimal micro-structures depending on the values assumed by the macro-variables. The stiffness tensors of the micro-structures are then used in the macro-scale optimization to assemble the global stiffness matrix K of the macro-structure. Subsequently, this matrix is inverted to solve the equilibrium problem $u = K^{-1}f$ and compute the global compliance c. The macro-design variables are iteratively updated until reaching the optimal values from which obtain the optimal macro-structure.

In the new developed approach, the mechanical properties of the cell can be determined through the classical solution of the strain and equilibrium problems following either Euler-Bernoulli's or Timoshenko's theory. However, since the relative density of the unit cell can also assume values approaching to one, the beam theory loses accuracy. Consequently, the behaviour of the unit cell is obtained by projecting it on a Finite Elements mesh and solving the equilibrium equations as Xia and Breitkopf [29] where an energy-based homogenization approach is adopted. The stiffness tensor is obtained in terms of element mutual energies by imposing three unit-strain tests to the unit cell as shown in Figure 3. They correspond to two normal strain fields and one shear strain field. The nodal displacements for each unit-strain test are computed applying the periodic boundary conditions [30]. To better understand the inverse homogenization method, the periodic boundary condition and the Matlab implementation the related papers are suggested [4,29,30].

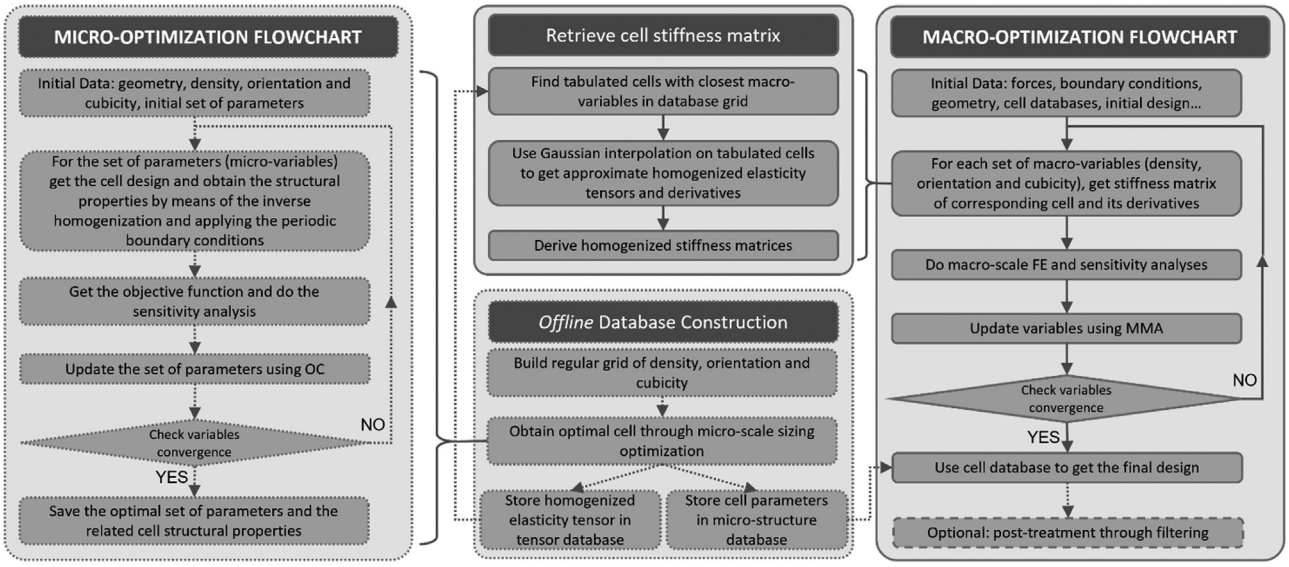

Fig. 4. Method flowchart.

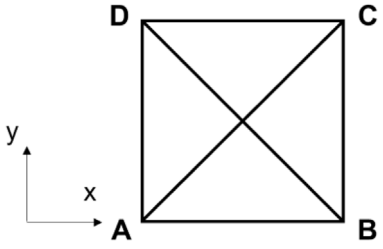

Fig. 5. Base unit cell with the beams AB, BC, CD, AD, AC and BD.

3 The new explicit approach

In this section the new explicit approach is explained starting from how the truss-based unit cells are built. The new micro-scale optimization and the definition of the lighter database are described. The macro-scale optimization is briefly reported too. In Figure 4 the flowchart diagram of the proposed method is shown.

3.1 Truss-based unit cell

The considered unit cell is made by superimposing a square structure and an x-shaped structure as illustrated in Figure 5, as Wang et al. [20], Wu et al. [31] and Zhang et al. [32]. This design allows to ensure an intrinsically well-connection between neighbouring cells, avoiding the definition of the transmission zones. In the meanwhile, 6 beams that connect the 4 vertices of the square design space can be identified: AB, BC, CD, AD, AC and BD.

The unit cell is moreover parametrized by 4 geometric parameters $\beta_i (i=1,2,3,4)$ that allow to cluster the beams in 4 "groups", each group being related to one of the β_i-parameters as described in Figure 6. These parameters are defined as the ratio between the actual thickness of the associated beams and the maximum physical thickness. Therefore, each parameter can range from 0 to 1. For example, considering the group (a) in Figure 6, the beams AD and BC can assume a thickness from 0 to half the side of the design space, in particular here β_1 is equal to 0.2.

The unit cell design is built starting from a full-white cell design and giving as inputs the dimensions of the cell and the values of the 4 parameters. As stated before, the thicknesses of the beams are related to the parameters. 4 vertices are defined for each element, as shown in Figure 7, and for each j-th vertex the distance d_j from the boundary (or the axes for the diagonal beams) of the beam is evaluated. The maximum and minimum distances are compared to the thickness t_i (or the half-thickness for the diagonal beams) of the i-th beam to understand if the element is completely covered, partially covered or not covered by the i-th beam. If the element is covered (as for element A, all the distances are less than t_1 that is the thickness of beam AD), the value 1 is assigned to its density, otherwise (as for element B, all the distances are greater than t_1) the value remains 0. If the element is partially covered (as for element C, d_1 or equally d_4 are less than t_1 and d_2 or equally d_3 are greater than t_1), a value from 0 to 1 has to be assigned in order to have a smooth curve for the volume fraction of the structure depending on the parameters. The value assigned is the area of the element covered by the beam; for the element C, since the beam occupy half element, the value assigned is 0.5 as shown in Figure 8, where the fictitious density of the element C is plotted with respect to the beam thickness. The designs of each group of beams are evaluated one by one independently, therefore, 4 values of fictitious density are associated to each element. Finally, the structure is obtained by keeping only the maximum fictitious density associated to each element. The design is represented with a grey scale, where white stands for a fictitious density 0, black for 1 and grey for the intermediate values. It is important to note that the grey elements can only appear at the border of the beams. These grey elements are

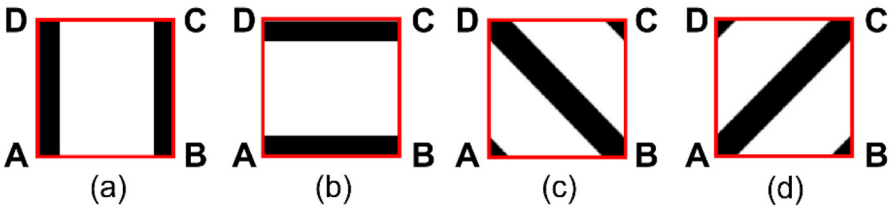

Fig. 6. The 4 β-dependent groups of beams. **(a)** AD and BC are defined by the parameter β_1; **(b)** AB and CD are defined by the parameter β_2; **(c)** BD is defined by the parameter β_3; **(d)** AC is defined by the parameter β_4. Here, the 4 designs are obtained by assigning the value 0.2 to the related parameter.

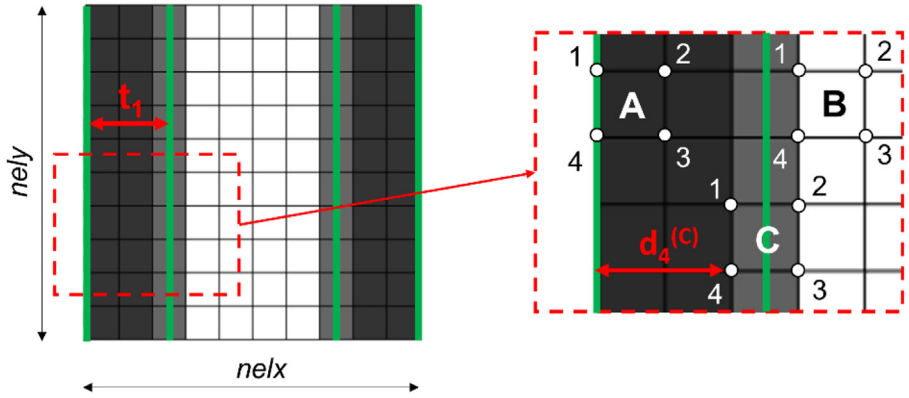

Fig. 7. Detail to understand the implementation for the unit cell: the element A is completely inside the beam so is black; the element B is completely outside the beam so is white; the element C is half covered by the beam, so the value assigned is 0.5 and is grey.

fundamental to have smooth partial derivatives of the objective function and the constraint with respect the parameters in the micro-optimization (Eq. 4 and Eq. 5).

The implemented Matlab function to build the unit cell can be called from the command window $x = Cell\_4p(nelx, nely, beta)$ where *nelx* and *nely* are the dimensions of the design space respectively along the x and y directions, and *beta* is the vector of the parameters $\beta = [\beta_1,\beta_2,\beta_3,\beta_4]$, the output x are the fictitious density of the elements of the design space. The design in Figure 7 is obtained by calling from the command window $x = Cell\_4p$ (10, 10, [0.5, 0, 0, 0]).

3.2 The micro-scale optimization

Once implemented the code for the structural architecture of the unit cell, the micro-optimization code is developed to compute the database of optimal micro-structures on a regularly-spaced 3-dimensional grid of the three macro-variables (density x_{dens}, orientation x_{or} and cubicity x_{cub} introduced in Sect. 2).

The design space is a discretized square of N ($= nelx \times nely$) micro elements. The design variables are the parameters β, that define the structure assigning to each element a fictitious density x_e (a value from 0 to 1) thanks to the unit cell code explained in Section 3.1. The Young's modulus of each micro element is given by a linear relationship with x_e:

$$E_e(x_e) = E_{min} + x_e(E_0 - E_{min}), \tag{1}$$

where E_e is the element Young's modulus, E_0 is the Young's modulus of the material and E_{min} is a very small stiffness assigned to void regions in order to prevent the stiffness matrix from becoming singular. A linear combination is used since the grey elements can only appear at the border of the beams and so it is not necessary to penalize them as the SIMP approach [33].

Once the structural architecture of the unit-cell is defined, the structural properties can be evaluated by means of the inverse homogenization and the periodic boundary conditions as in Xia and Breitkopf [29]. In this work, an energy-based homogenization approach allows to obtain the 4-th order homogenized stiffness tensor $(\boldsymbol{E}_{klqp})_{k,l,q,p\in\{1,2\}}$ of the unit-cell by the equation (2).

$$\boldsymbol{E}_{klqp} = \frac{1}{N}\sum_{i+1}^{N} (u_i^{A(kl)})^T k_i u_i^{A(pq)}, \tag{2}$$

where N is the number of micro elements, k_i is the stiffness matrix of the i-th micro-element, and $u_i^{A(pq)}$ are the displacement solutions for the for i-th micro-element corresponding to the unit-test strain fields in Figure 3 applied to the considered unit-cell. In Figure 3 the unit-test strain corresponds to $(p,\ q) = (1,\ 1)$, $(2,\ 2)$ and $(1,\ 2)$.

Therefore, the stiffness tensor is equal to

$$\boldsymbol{E} = \begin{bmatrix} E_{1111} & E_{1122} & E_{1112} \\ E_{2211} & E_{2222} & E_{2212} \\ E_{1211} & E_{1222} & E_{1212} \end{bmatrix},$$

Following the original EMTO, the objective function $e(\beta)$ is defined as the weighted sum of the two principal components of the homogenized stiffness tensor rotated of an angle α as follows

$$e(\beta) = -\left[\left(1 - \frac{\sqrt{x_{cub}}}{2}\right)\boldsymbol{E}_{1111}^{\alpha(x_{or})}(\beta) + \frac{\sqrt{x_{cub}}}{2}\boldsymbol{E}_{2222}^{\alpha(x_{or})}(\beta)\right], \quad (3)$$

where α $(= x_{or}\pi/4)$ is related to the orientation macro-variable x_{or} belonging to the interval [0,1], the weights depend on the cubicity macro-variable x_{cub} belonging to the interval [0,1] and the rotated stiffness tensor $\mathbf{E}\boldsymbol{\alpha}$ is obtained using the following equation

$$\boldsymbol{E}^{\alpha} = \boldsymbol{M}_{\alpha}^{T} \times \boldsymbol{E} \times \boldsymbol{M}_{\alpha} \equiv \left(\boldsymbol{E}_{klpq}^{\alpha}\right)_{k,l,p,q\in[1,2]},$$

where $\mathbf{M}_{\alpha}$ is a rotation tensor defined for a rotation angle α measured with respect to a chosen global basis vector. For example, assuming $x_{or} = 0$ (that stands for an angle $\alpha = 0$) and $x_{cub} = 0$, the objective function becomes $e(\beta) = -\mathbf{E}_{1111}$ and the optimization procedure is going to search for an optimal micro-structure with the highest possible first principal component respecting the volume fraction constraint given by x_{dens}.

Therefore, the mathematical formulation of the micro-optimization problem for the unit-cell is

minimize

$$\beta_j, j = 1...4 \quad e = -\left[\left(1 - \frac{\sqrt{x_{cub}}}{2}\right)E_{1111}^{\alpha(x_{or})} + \frac{\sqrt{x_{cub}}}{2}E_{2222}^{\alpha(x_{or})}\right]$$

subject to

$$F(p,q) = Ku^{A(p,q)}$$

$$\frac{V(\beta)}{V_0} = v \geq x_{dens}$$

$$0 \leq \varepsilon \leq \beta_j \leq 1\, j = 1...4.$$

Here K is the unit-cell assembled stiffness matrix, u^A and F are the global displacement vector and the external force vector of the unit-cell, $V(\beta)$ is the volume occupied by the material, V_0 is the total volume of the design space, ν is the material volume fraction, β_j are the parameters whose lower bound is a very small value ϵ and the upper bound is

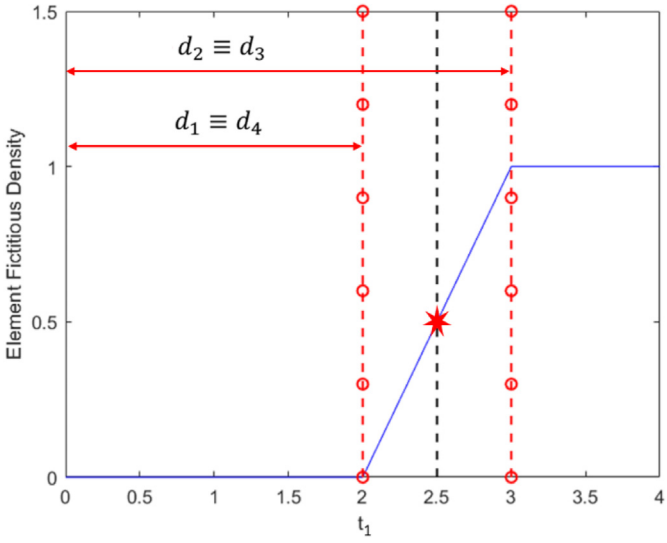

Fig. 8. Fictitious density plot depending on the thickness t_1 considering the element C from the example in Figure 7. The distances d_1 (that is equal to d_4) and d_2 (that is equal to d_3) are reported with red dot-dashed lines, t_1 is set along vertical black dashed lines and the fictitious density for t_1 is reported with a red star in the graph.

1. The micro-optimization of the new approach is not a topology optimization as for the original EMTO, but is a sizing optimization.

The sensitivity analysis is carried out by finite differences for both the objective function e and the constraint v for simplicity, since the analytic derivates are not easy to compute. For each j-th parameter, the following derivatives are evaluated.

$$\frac{\partial e}{\partial \beta_j} \cong \frac{e(\beta_j + h) - e(\beta_j)}{h}, \quad (4)$$

$$\frac{\partial v}{\partial \beta_j} \cong \frac{v(\beta_j + h) - v(\beta_j)}{h}. \quad (5)$$

Once the derivatives are obtained, the optimality criteria method (OCM) is used to solve the optimization problem with the heuristic updating scheme following Sigmund [34].

The iterative process terminates when the difference for each j-th parameter $\beta_j^{new} - \beta_j$ is less than the convergence tolerance 10^{-5}, when 150 iterations are reached, or when 50 iterations without finding a new minimum are reached.

The Matlab function can be called by the command window as follows

$$[tens, obj, beta] = unitCell\_4p(nelx, nely, x\_dens, penal, x\_or, x\_cub, beta\_0)$$

$$E = \begin{bmatrix} 0.24 & 0.11 & -0.11 \\ 0.11 & 0.13 & -0.12 \\ -0.11 & -0.12 & 0.13 \end{bmatrix}$$

$$E^{\alpha} = \begin{bmatrix} 0.47 & 0.05 & -0.08 \\ 0.05 & 0.02 & 0.00 \\ -0.08 & 0.00 & 0.07 \end{bmatrix}$$

Fig. 9. Example of optimal unit cell for $x_{dens} = 0.55$, $x_{or} = 0.63$ (α of about $\pi/6$) and $x_{cub} = 0.31$. The stiffness tensor and the rotated stiffness tensor are shown too.

here *nexl* and *nely* are the dimensions of the design space respectively along the x and y directions, *x_ dens*, *x_ or* and *x_ cub* are the macro-variables, *penal* is the penalization coefficient (set to 1) and *beta_ 0* is the initial guess vector of the parameters β. The outputs are the homogenized stiffness tensor, the objective function and the vector of the parameters named respectively *tens*, *obj* and *beta*.

For illustration, let us consider a random example with a 100×100 initial full white design space (*beta_ 0* = [0,0, 0, 0]) and for $x_{dens} = 0.55$, $x_{or} = 0.63$ (that corresponds to an orientation angle α of about $\pi/6$) and $x_{cub} = 0.09$. The obtained structure with the related stiffness tensor $\mathbf{E}$ and rotated stiffness tensor $\mathbf{E}^{\alpha}$ are shown in Figure 9. The optimal unit cell is found at the 61-th iteration and both the objective function e and the volume fraction v rapidly reach the optimal point after 15 iterations, as shown in Figure 10, with the vector of the parameters equal to $\beta = [\beta_1, \beta_2, \beta_3, \beta_4] = [0{,}0.11, \quad 0.49, \quad 0]$ and the objective function $e = -\left[\left(1 - \frac{\sqrt{x_{cub}}}{2}\right)\boldsymbol{E}_{1111}^{\alpha(x_{or})} + \frac{\sqrt{x_{cub}}}{2}\boldsymbol{E}_{2222}^{\alpha(x_{or})}\right] \cong -0.4005$.

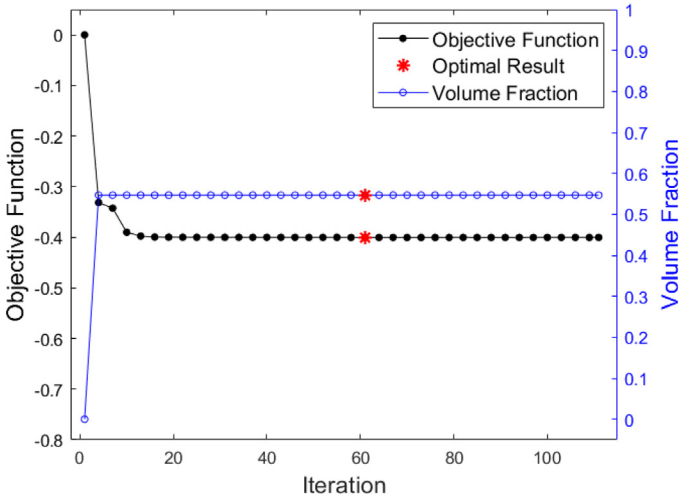

Fig. 10. Iteration history for the example in Figure 9.

3.3 The macro-scale optimization

Before presenting the new database and the results obtained, a brief explanation of the macro-scale optimization is given without going too much in the implementation details. We refer to Duriez et al. [28] for a more detailed description.

For a design space of M macro-elements, the objective function is the compliance of the structure, and the design variables are the density, orientation and cubicity explained in Section 2, named in the code respectively x_{dens}, x_{or} and x_{cub}. Therefore, each macro-element has three variables assigned during the optimization process. The problem formulation is

$$\begin{aligned} &\text{minimize} \\ &x = [x_{dens}, x_{or}, x_{cub}] \quad c(x) = U^T K U \\ &\text{subject to} \quad F = KU \\ &\qquad \sum_{j=1}^{M} x_{dens}^{j} \leq M f_v \\ &\qquad 0 \leq x^j \leq 1, j = 1 \ldots M, \end{aligned}$$

where U is the global displacements matrix, K is the stiffness matrix, F is the vector of the external forces and f_v is the volume fraction constraint.

Actually, due to the periodicity of the orientation variable, the applied filtering method [33] could lead to optimization issues. To mitigate these issues, the orientation variable x_{or} is replaced by two other variables, from which the orientation is derived:

$$x_{or} = arctan\left(\frac{x_{sin}}{x_{cos}}\right),$$

where x_{sin} and x_{cos} are not the real sine and cosine but have the same ratio. Defining these variables allows to make the design space redundant, since any set of x_{sin} and x_{cos} with the same ratio corresponds to the same orientation.

During the optimization the stiffness tensor of the j-th macro-element is obtained from the database for the set $\left[x_{dens}^{j}, x_{or}^{j}, x_{cub}^{j}\right]$ by using the Nadaraya-Watson's kernel-weighted average [35] obtaining $\boldsymbol{E}_{pred}(x^j)$ and its derivatives with respect to the design variables. The surrogate prediction of $\boldsymbol{E}_{pred}(x^j)$ is reported in Appendix A. E_{pred} enables to find the stiffness matrix K and to solve the equilibrium equation by a finite element analysis. After the

sensitivity analysis, the variables are updated with the method of moving asymptotes (MMA, [36]) and the convergence is checked. The process goes iteratively ahead until one of the termination criteria is satisfied: 100 maximum number of iterations, 15 maximum number of iterations without a new minimum or 10^{-3} convergence tolerance. Finally, the macro variables and the compliance of the final design, computed using the homogenized stiffness tensors, are obtained as outputs.

Once obtained the final optimal set of macro variables for each macro element, the full scale structure can be obtained by replacing each macro-element with the closest cell in terms of Euclidean distance in the micro-structure database. Due to the limits of using homogenization to obtain the overall compliance of the final structure, the full-scale structure can be evaluated by computing the compliance with a finite element analysis. The EMTO also includes the possibility to use a post-processing code to improve the structure performances by assuring connection between micro-structures and getting rid of unstressed elements. The post-processing consists in three steps. In the first step, a full finite element analysis is carried out on the design to compute the stress in all the micro-elements. These stresses are compared to the mean stress value through the structure times a given constant C_{post} to assess if the elements are or not useful. If they are lower than C_{post} times the mean stress value, the related element is "deleted" setting density to 0. The process is repeated three times considering three different constants. In the second step, a classical density filter is applied having a filter radius defined with respect to the micro-element size, improving manufacturability and making the thin structural members thicker. Then, all the elements are set to a density value 0 or 1 depending on a threshold that is adjusted through an iterative process to ensure the desired volume fraction. The final step gives the full-scale final design. The original EMTO work [28] is suggested to have further details about the post-processing.

3.4 Database construction

The database is constructed off-line in order to have a faster macro-optimization. The inputs of the database are the three macro-scale design variables and the outputs are the four parameters to build the cell and the six independent terms of the homogenized stiffness tensor of the corresponding cell. Actually, the database is divided into two databases, one containing the tensors, and the second one the parameters. Only the tensors are loaded during the macro-optimization. Once the macro-optimization is finished, the database of parameters is used to get the full-scale design by calling the unit-cell code in Section 3.1.

The database is computed considering cells of 100×100 elements for the 3-dimensional grid as in Figure 11 whose coordinates are given by:

– 32 values from 0 to 1 (0 and 1 excluded) for the volume fraction (density variable);

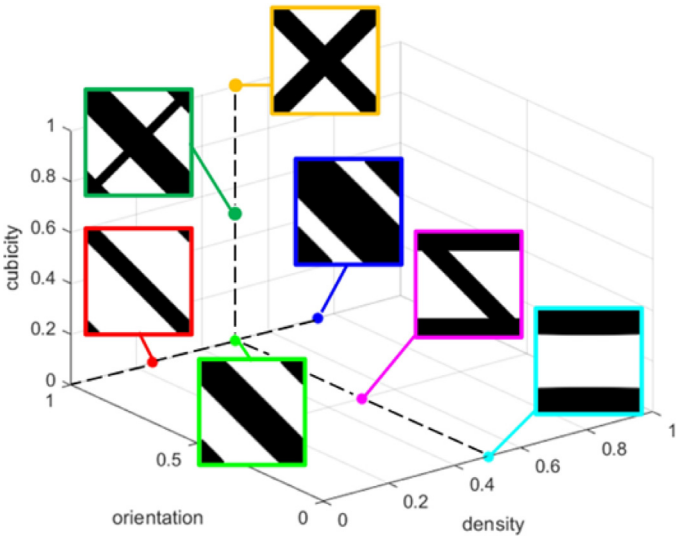

Fig. 11. The 3-dimensional grid over which the database is computed. Some cells are shown to show the effects of the three macro-variables.

– 32 values from 0 to 1 for the orientation variable (or equally angle α), where 0 stands for a rotation angle of 0 *rad* and 1 for a rotation angle of $\pi/4$ *rad*;
– 32 values from 0 to 1 for the cubicity variable, where 0 stands for stiffness only along the first principal direction and 1 for equal stiffness along both directions.

Considering a multi-start strategy with 4 possible initial guesses, the total number of designs evaluated is equal to $32^3 \times 4 = 131072$. The best solution for each input combinations is kept and added to the database. The unit cells for volume fractions 0 and 1, computed only once because they correspond to void and full material unit cells, are added too. So, a first database containing 34816 unit-cells and their properties is obtained.

Since the original EMTO follows SIMP with penalization $p = 3$ to obtain the optimal unit-cells, to compare the parametrized cells of the Ex-EMTO with the free ones of the original EMTO, the properties and the objective functions for the parametrized cells in Figure 12 have been recomputed by considering a penalization $p = 3$. The worsening of the performances of the parametrized cells due to the introduction of the penalization is very low since the grey elements can only appear at the border of the beams as explained in Section 3.1. In fact, considering a sample group of 3584 very different cells, the mean deviation of the objective function computed with $p = 3$ with respect to the ones with a linear relationship for the Young's modulus (that can be seen as having $p = 1$) is about 2.5%.

The unit cells obtained with the parametrized approach have more regular shapes than the free cells by the original EMTO as shown in Figure 12. Due to the parameterization, the design space is restricted and the performances are worse: the objective function value increases by about 2-10%. However, it is an acceptable trade off to diminish the

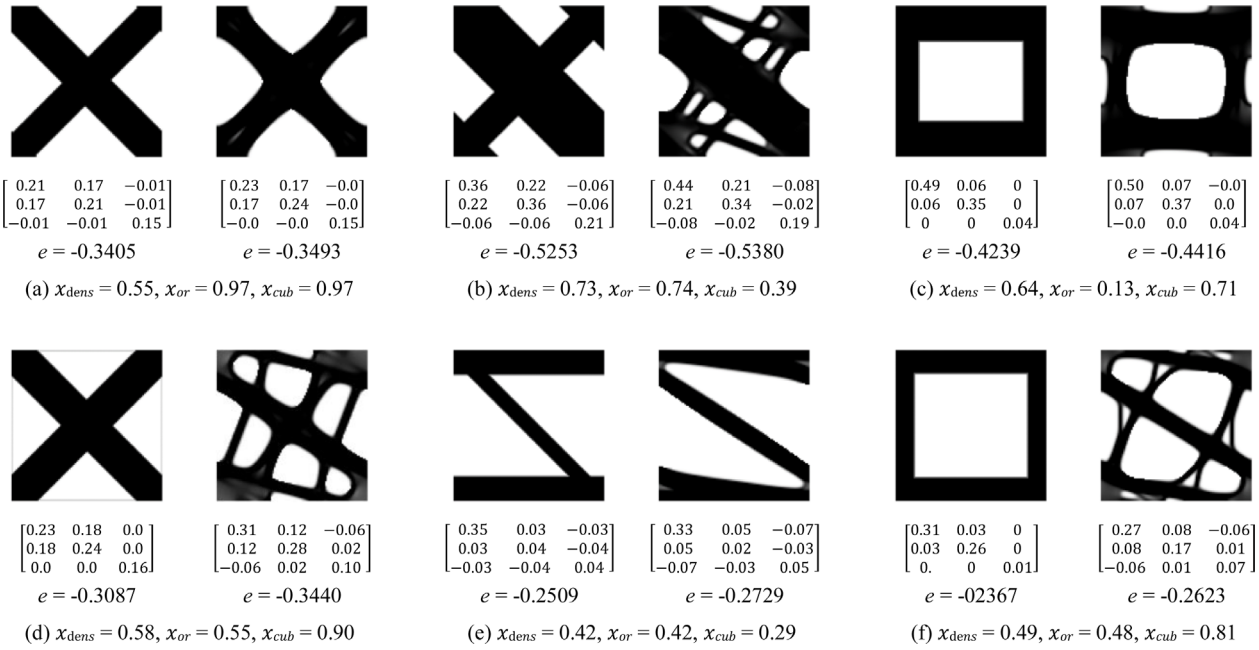

Fig. 12. Random examples of cells with the related homogenized stiffness tensor and objective functions from the new database (left) compared to the ones from the original EMTO database (right). The orientation variable from 0 to 1 means an orientation angle from 0 *rad* to $\pi/4$ *rad*; the cubicity variable ranges from 0 to 1, where 0 stands for stiffness only along the first principal direction and 1 for equal stiffness along both directions.

database size of about the 97% since the structure database needs to store just the 4 parameters $\beta = [\beta_1, \beta_2, \beta_3, \beta_4]$ and not the N micro-elements of the structure.

Besides, the design space has to be artificially extended to avoid local minima at the border. Therefore, the database is extended by applying symmetries and rotation to the computed unit cell without the need of solving further micro-optimization problems. The final database contains unit cells for an orientation variable ranging from 0 to π *rad* (redefining x_{or} from 0 to 1) and *cubicity* variable from stiffness only along the first principal direction considered (value 0) to stiffness only along the second principal direction (value 1), whereas a value of 0.5 means that stiffness is along both the principal directions. Finally, the final database is obtained with a total number of unit cells equal to 267750. In this way, the gradient-based macro-optimizer has multiple paths from a cell to another as shown in Figure 13.

Due to the restricted unit-cell design space, the transition from one cell to another by changing only one macro variable is not always smooth, as shown in Figure 13b. In that figure, the three intermediate unit cells are almost equal and before and after them there is a quite sharp change to different cells. Despite this, the cells result to be well connected without the need to define the transmission zones.

4 Results and discussion

Classical test cases from the literature as shown in Figure 14 are solved with the Ex-EMTO approach and the results are analysed and discussed hereafter compared to the one of the original EMTO. The computational times are not reported since they are almost the same of the original EMTO ones [28]. This is related to the fact that the two approaches have in common the macro-optimization code and the two databases are structured in the same way. A test case for a comparison with another multi-scale approach is analysed too. For all the cases, the Young's modulus for the solid material is $E_0 = 1$, the Poisson's ratio 0.3 and the force $F = 1$.

4.1 MBB beam

In Figure 14a just half of the MBB problem is represented and considered for the computation thanks to the problem symmetry. A 30×10 macro-scale grid is considered. The objective is to minimize the compliance of the macro design with a constraint for the global volume fraction of 0.5. For both the EMTO and Ex-EMTO, the full-scale designs over a micro-scale grid 3000×1000 are obtained for a penalization coefficient $p = 3$ without and with the post-processing (PP) and are shown in Figure 15.

The designs are similar and, despite the worse performances of the unit cells of the new Ex-EMTO database, the compliances are almost equal too, as can be seen in Table 1. In that table, the objective functions and the %-variation with respect to the "homogenized" compliance (the one obtained by the computation by using the stiffness tensors from the database) of EMTO are reported for each step of the optimization. By comparing Figures 15a and 15c, the limitation of the new approach is evident for the cells where there is a transition from normal

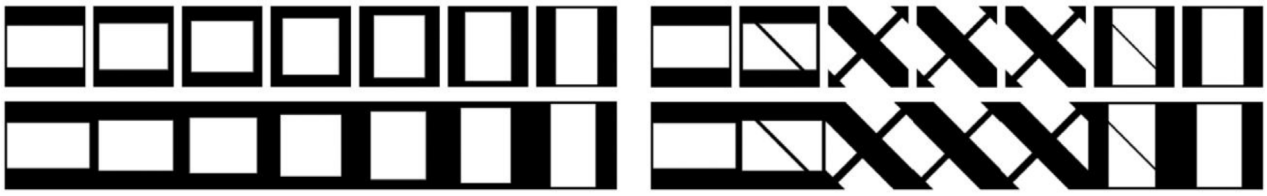

(a) Micro-structures obtained for density = 0.5, orientation angle α = 0 *rad* and extended *cubicity* values ranging from 0.2 to 0.8.

(b) Micro-structures obtained for density = 0.5, orientation angle ranging from 0 *rad* to $\pi/2$ *rad* and extended *cubicity* equals to 0.2.

Fig. 13. Unit cells examples to show the redundant design space. There are two paths from the cell on the left (density = 0.5, orientation = 0 *rad*, cubicity = 0.2) to the cell on the right ((a) density = 0.5, orientation = 0 *rad*, cubicity = 0.8 or (b) density = 0.5, orientation = $\pi/2$ *rad*, cubicity = 0.2).

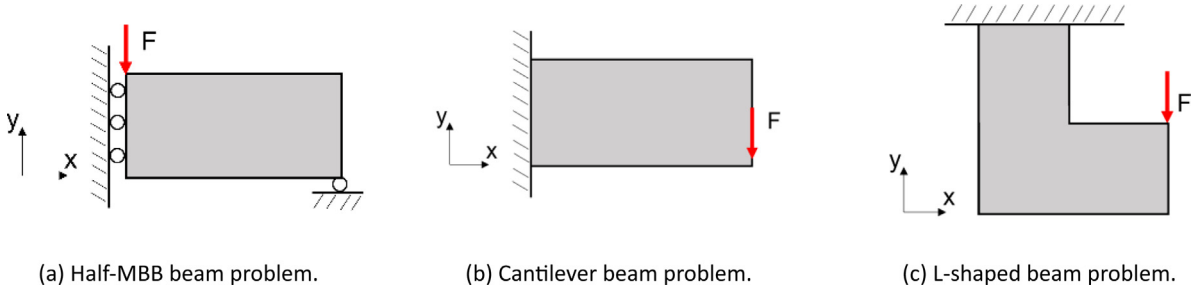

(a) Half-MBB beam problem. (b) Cantilever beam problem. (c) L-shaped beam problem.

Fig. 14. Beam problems.

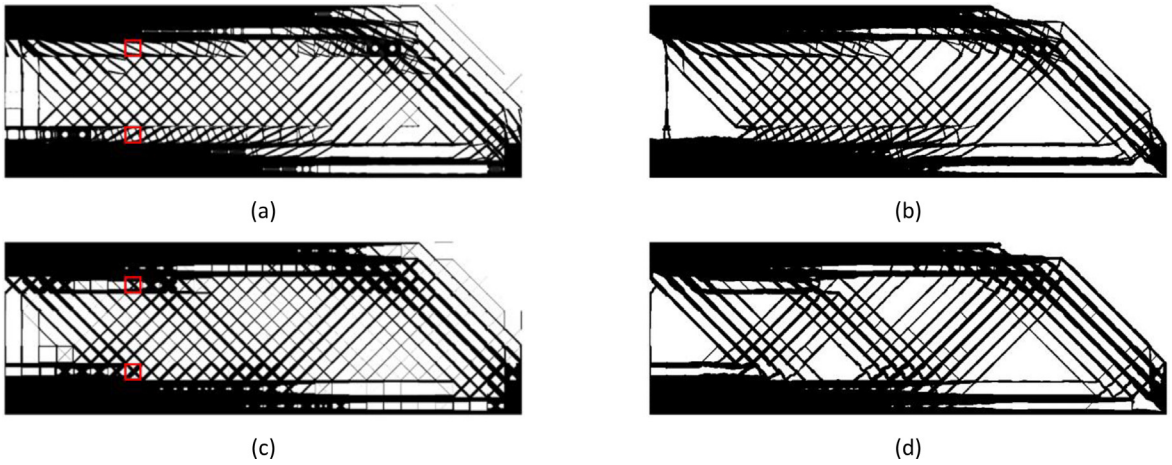

Fig. 15. Comparison of MBB designs with 100 × 100 cells for the compliance minimization: (a) and (b) original EMTO respectively without post-processing and with post-processing, (c) and (d) Ex-EMTO respectively without post-processing and with post-processing.

stress to shear stress (for example the cells highlighted in red). In fact, as anticipated in Section 3 with Figure 13, the restricted design space of the parametrized cells does not allow to obtain optimal cells for transition stress cases as good as the free cells. Moreover, after the post-processing in Figure 15d (Ex-EMTO) those cells are slightly distorted, whereas in Figure 15b (EMTO) they are almost the same as before the post-processing. However, the performances of Ex-EMTO are only diminished by 1% with respect to the ones of original EMTO, meaning that the previous limitation is not detrimental. In addition, the fact that the performances are similar between original EMTO and Ex-EMTO, demonstrates that the parametrized unit cells are intrinsically well-connected as expected. Moreover, the convergence performances are similar too as shown for the homogenized step in Figure 16. Both the codes have a rapid drop for the compliance before the 15-th iteration and then converges to a final value approximately equal, instead the volume fraction is quite regular. EMTO converges after 67 iterations, Ex-EMTO after 90 iterations.

Table 1. Comparison of compliances from EMTO vs Ex-EMTO for the MBB beam problem for the different steps in the method.

Step	Evaluation grid	Objective function c	vs EMTO-Homo
EMTO			
Homogenized	30×10	193.8	–
No PP - 100×100 cells	3000×1000	213.1	+ 10.0%
PP - 100×100 cells	3000×1000	203.6	+ 5.1%
No PP - 25×25 cells	750×250	214.0	+ 10.4%
PP - 25×25 cells	750×250	200.1	+ 3.3%
Ex-EMTO			
Homogenized	30×10	192.7	– 0.0%
No PP - 100×100 cells	3000×1000	212.1	+ 9.4%
PP - 100×100 cells	3000×1000	205.7	+ 6.1%
No PP - 25×25 cells	750×250	214.8	+ 10.8%
PP - 25×25 cells	750×250	202.2	+ 4.3%

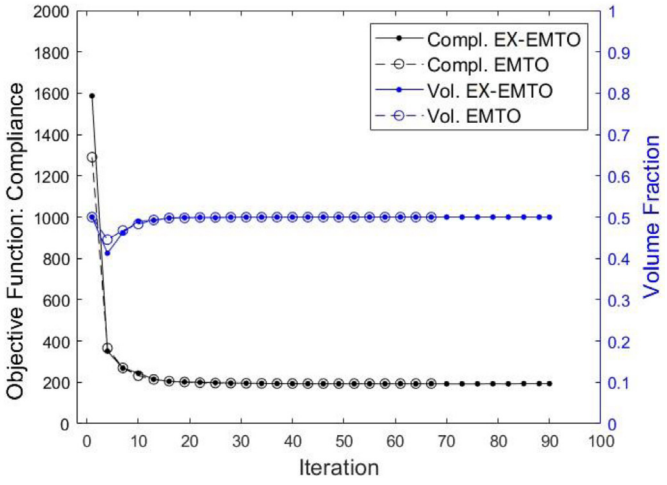

Fig. 16. Homogenized step iteration histories for the MBB beam.

4.2 Cantilever beam

The cantilever beam is shown in Figure 14b and a 20×10 macro-scale grid is considered. The objective is to minimize the compliance with a constraint for the global volume fraction of 0.5. Both the EMTO and the Ex-EMTO full-scale designs over a 2000×1000 micro-scale grid without and with post-processing are shown in Figure 17. As for the MBB beam problem, the cantilever beam designs are similar but the performances with the new database are worse of only the 3% with respect to the one of the original EMTO, as reported in Table 2. The difference in the performances between EMTO and Ex-EMTO are higher for the cantilever beam than for the MBB beam, but they are still small. This is probably due to the limitation of the parametrized unit cell, as in the MBB beam design, for the "transition" cells. Therefore, the observations are similar to the MBB beam ones. However, for the cantilever beam, the designs with the post processing (Figs. 17b and 17d) results to be almost equal to the "homogenized" step ones. In Figure 18, the iteration histories for the homogenized step are shown for both the code. The compliance rapidly drops before the 10-th iteration, instead the volume fraction shows a less regular behaviour until the 25-th iteration. The final convergence is reached for both the code after the 95-th iteration.

4.3 L-shaped beam

The L-shaped beam problem in Figure 14c with a 14×14 macro-scale grid is considered. The objective is to minimize the compliance with a volume fraction constraint of 0.5. The full-scale designs over a 1400×1400 micro-scale grid are shown in Figure 19. The designs obtained by Ex-EMTO show more regular shapes and have performances comparable with the ones of EMTO as reported in Table 3 and shown in Figure 20. However, both the approaches for the full-scale designs have performances worse by more than 20% with respect to the "homogenized" step. This discrepancy is due to the low number of macro-elements used to be able to compute the full-scale model. Consequently, the loads are not perfectly transmitted from one cell to another. Using more macro-elements would give lower discrepancies.

4.4 Comparison with works from literature

Ex-EMTO has been tested also for a half MBB beam problem with a macro-scale grid 32×24 and 0.3 global volume fraction constraint to compare the results with the ones obtained for the same problem by Garner et al. [17]. The design obtained by Garner in Figure 21a has been projected over a micro-scale grid of 800×600 as in Figure 21b and the compliance evaluated with the same code used to evaluate the full-scale designs of the EMTO. For the comparison, the original EMTO has been considered too. To reduce the computational and memory efforts of EMTOs, the 100×100 cells of the databases have

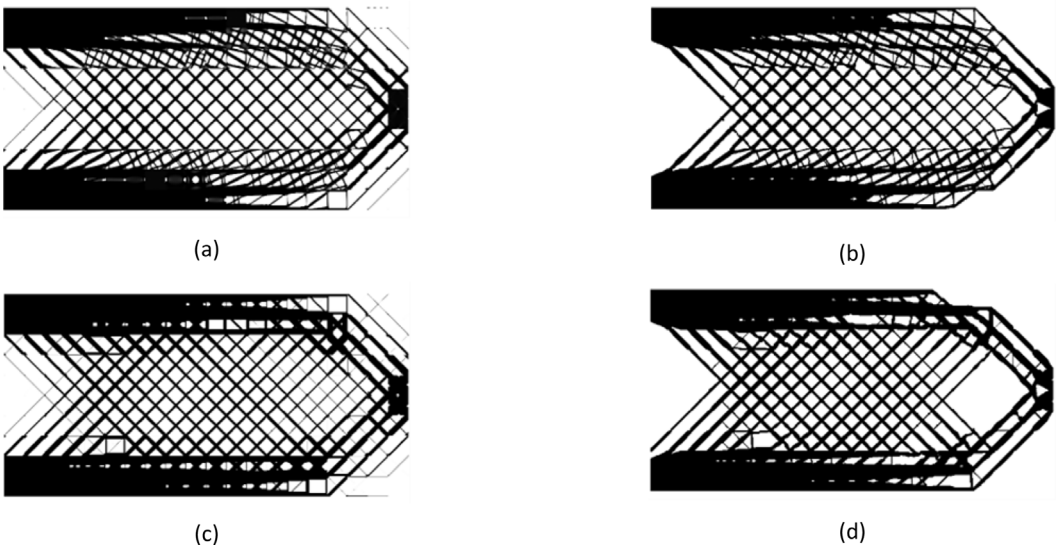

Fig. 17. Comparison of Cantilever beam designs which minimize the compliance: (a) original EMTO without post-processing, (b) original EMTO with post-processing, (c) Ex-EMTO without post-processing and (d) Ex-EMTO with post-processing.

Table 2. Comparison of compliances from EMTO vs Ex-EMTO for the Cantilever beam problem for the different steps in the method.

Step	Obj. function c	vs EMTO-Homo
EMTO		
Homogenized	67.6	–
No PP	72.8	+7.7%
With PP	67.5	−0.0%
Ex-EMTO		
Homogenized	67.8	+0.0%
No PP	74.4	+10.1%
With PP	69.5	+2.8%

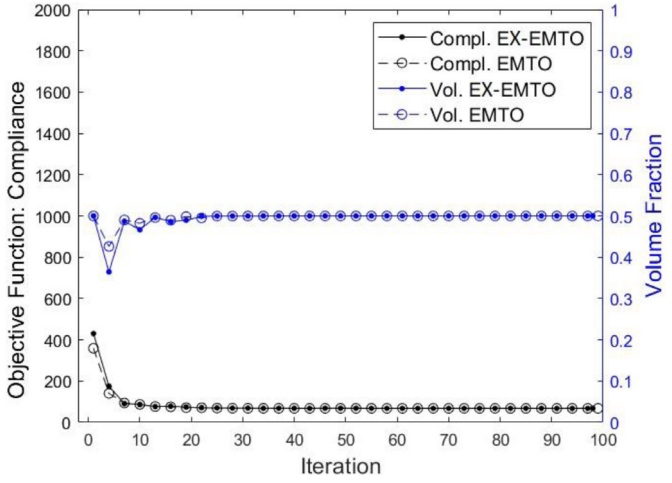

Fig. 18. Homogenized step iteration histories for the Cantilever beam.

been reshaped to 25×25 cells, allowing also to have the same micro-scale grid of 800×600 elements. It is immediate to reshape the parametrized cells since the code to build the cells allows to do that by inserting as input the desired dimensions and the vector of parameters (stored in the database). In Figure 22, some reshaped cells both for Ex-EMTO and original EMTO, with their stiffness tensors and objective functions, are shown. The parametrized cells are less affected by the reshaping, as can be seen by comparing the objective function values of the cells in Figure 12 with the reshaped cells in Figure 22. This is probably due to the much more regular shapes of the parametrized cells as can be seen in Figures 22b and 22c. Considering 3584 cells, the reshaping leads to a mean worsening of the objective function of about 5.8% for the parametrized cells and 6.9% for the free cells. Despite the loss in performance of the unit cells, substituting in the full scale design the reshaped cells (for example the 25×25 cells instead of the 100×100 cells) does not affect the results in terms of compliance as shown for the half MBB problem in Table 1 in Section 4.1. However, since the database of the stiffness tensors is related to the 100×100 cells, full scale results with reshaped cells in line with the "homogenized" step ones are not always sure.

In Table 4 the compliances of the various designs are reported and compared to the ones of top88 (mono-scale approach) with the 800×600 grid. The designs of top88 (on a 32×24 grid and 800×600 grid) are shown in Appendix B in Figure B1. As expected from the previous test problems Ex-EMTO and EMTO have similar results for each step of the methods. Both the EMTOs show an "homogenized" compliance lower of about the 12% with respect to the one of top88 on an 800×600 grid. However, after the introduction of the cells, obtaining the full-scale designs with the post-processing, the compliance for the EMTOs is slightly worse than the one of top88, about 5% worse, but

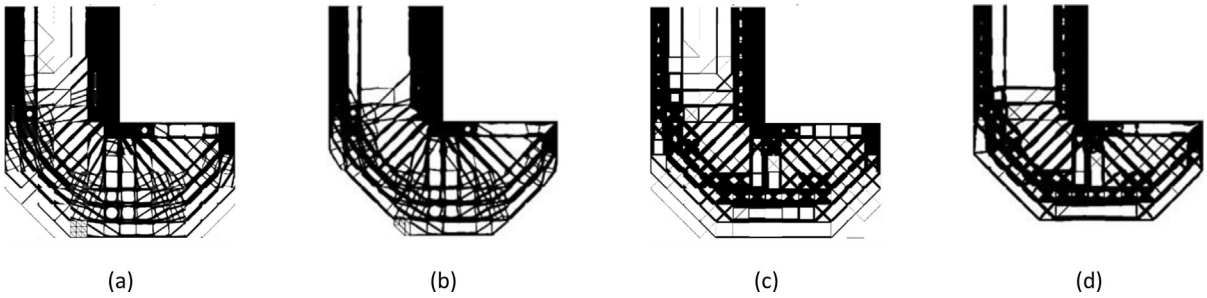

Fig. 19. Comparison of L-shaped beam designs which minimize the compliance: (a) original EMTO without post-processing, (b) original EMTO with post-processing, (c) Ex-EMTO without post-processing and (d) Ex-EMTO with post-processing.

Table 3. Comparison of compliances from EMTO vs Ex-EMTO for the L-shaped problem for the different steps in the method.

Step	Obj. function c	vs EMTO-Homo
EMTO		
Homogenized	78.2	–
No PP	106.0	+35.5%
With PP	95.9	+22.6%
Ex-EMTO		
Homogenized	78.5	+0.4%
No PP	106.4	+36%
With PP	97.6	+24.8%

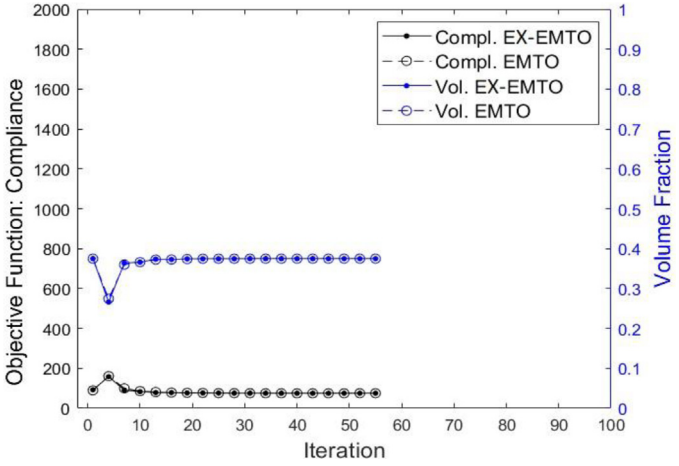

Fig. 20. Homogenized step iteration histories for the L-shaped beam.

with a lower computational effort and time as discussed in the previous work [28]. The total computational time to obtain and evaluate the EMTO full-scale design with the post-processing (800×600 grid) is about 6 times lower than the top88 time on the same 800×600 grid.

The post-processed designs deviate from the theoretical results of about the 16%, that is considered acceptable. This deviation with respect to the theoretical results could be also due to the reshaping of the cells. Therefore, designs with higher resolutions for the unit cells should be tested to find a lower limit for the dimensions of the cells reshaping. Despite the slightly worse performances of the EMTOs with respect to the top88 method, the results are instead much better than the ones obtained by Garner's method.

The previous comparisons and the new approach for the EMTO demonstrate the validity and versatility of the method. The introduction of the macro variables and the database allow to have a lot of freedom in the design of the unit cells. It is possible to reduce the solution space over which the database is built or to reduce the resolution of the unit cells without losing too much in the performances of the method.

4.5 Ultra-light design

Ultra-light structures are of great interest in several industries like automobile, aerospace and aircraft, and to get such structures, ultra-light materials are widely studied, including truss-like materials [37,38]. The Ex-EMTO allows to get truss-like ultra-light designs with very simple shapes. It has been tested for a 20×10 half MBB beam problem for compliance minimization with volume fractions 0.126, 0.127 and 0.128. The post processed designs, shown in Figure 23, are obtained with 50×50 cells, so over a 1000×500 micro-scale grid, and compared with the one of the original EMTO. The compliances are reported below each structure.

Thanks to the more regular shapes of the parametrized cells, the designs by Ex-EMTO results to be very simple and well connected. Moreover, the designs of the Ex-EMTO have better performances with respect to the one of the original EMTO since the compliances are much lower as can be seen from Figure 23. In particular, in Figure 23a the compliance of the new approach is about the half of the original one. The Pareto curve of the half MBB beam problem is shown in Figure 24.

5 Demonstration of the versatility of Ex-EMTO

The new Ex-EMTO approach to build the database demonstrates the versatility of the EMTO to be used with different types of unit cells. The versatility of the method is

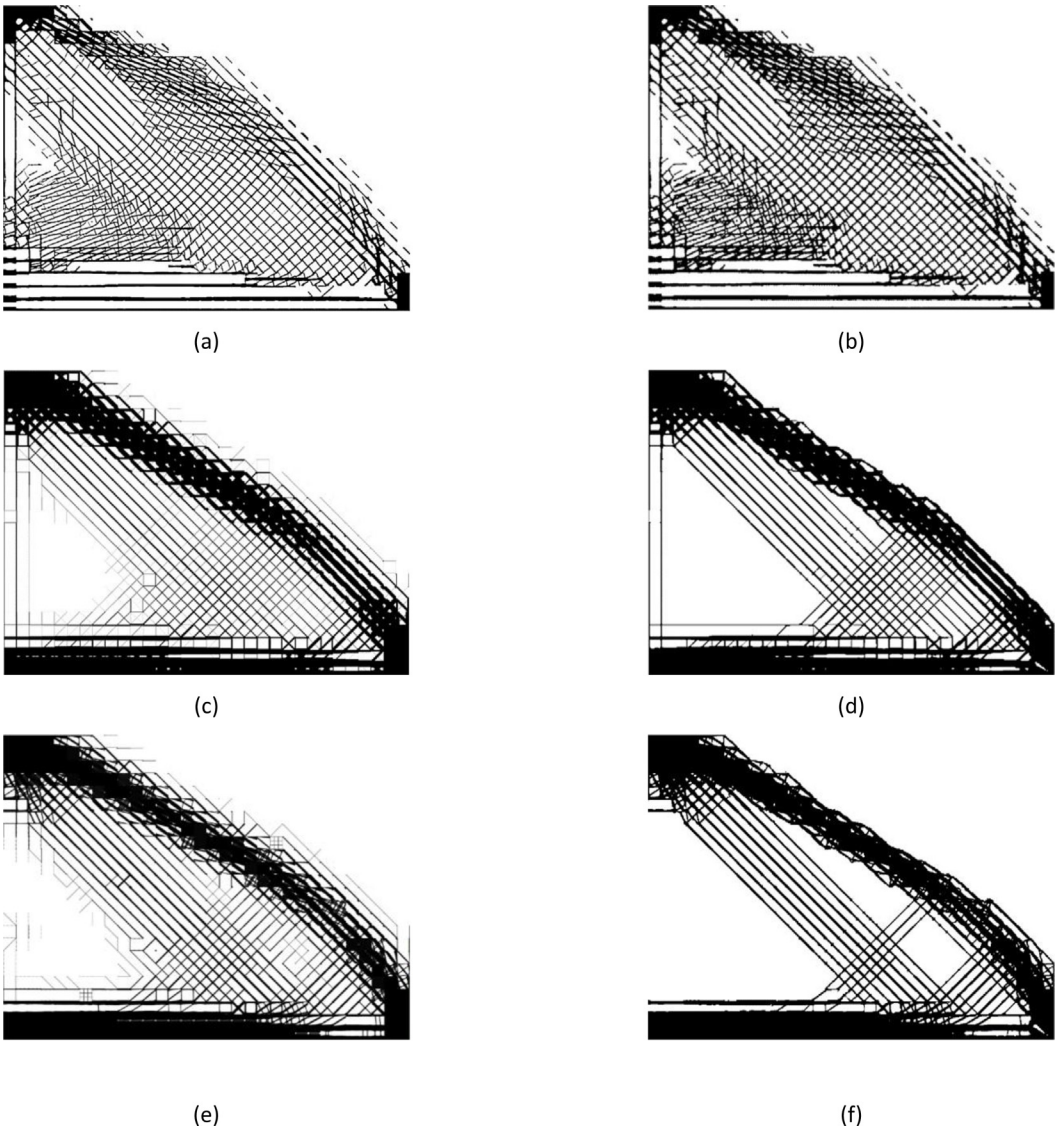

Fig. 21. Comparison of half MBB designs. (a) and (b) design from Garner et al. [17] and the same design reprojected on a 800×600 grid, (c) and (d) Ex-EMTO on a 32×24 grid of 25×25 cells (800×600 micro-scale grid) without and with post-processing respectively, (e) and (f) EMTO on a 32×24 grid of 25×25 cells (800×600 micro-scale grid) respectively without and with post-processing.

also related to the possibility to accommodate different types of problems and constraints. Therefore, it is interesting to see how these two strengths of the methods can coexist, by solving with the new database the problems of fiber orientation, controlled porosity [39] and fixed topology test cases.

5.1 The fiber orientation test case

Since one of the macro-variables is the orientation of the unit cell, EMTO can be easily adapted to get optimal fiber orientation in a topology optimization framework. In Figure 25, the orientations solutions for 80×40 half MBB beam problems are shown.

In Figure 25a, the problem has a constraint related to the usage of macro elements in percentage, that is set to 1, and a constraint for the unit cell volume fraction set to 0.5. Therefore, the global volume fraction constraint can be obtained by multiplication of the two constraints giving as a result 0.5. The images are the results of the Ex-EMTO (top) and the original EMTO (bottom) and show the orientation variable database indexes of each cell. The indexes go from 1 to 32, where 1 stands for 0 *rad* and 32 for $\pi/4$ *rad*. Ex-EMTO shows a smoother and more regular transition of the orientation variable.

In Figure 25b the problem the usage of macro elements in percentage is equal to 0.5 and the unit cell volume fraction 0.5, therefore a global volume fraction constraint of 0.25. In this case, the Ex-EMTO shows a better topology and also, as a consequence, a more regular orientation variation. These results are just preliminary results and further improvements are needed to correctly solve the fiber orientation test case.

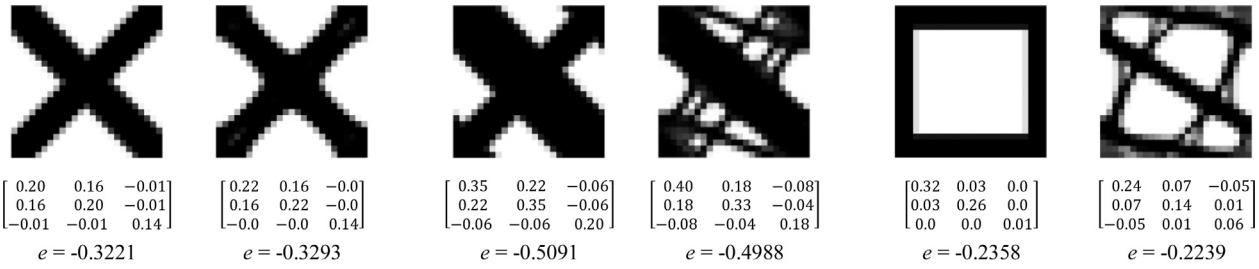

(a) $x_{dens} = 0.55$, $x_{or} = 0.97$, $x_{cub} = 0.97$ (b) $x_{dens} = 0.73$, $x_{or} = 0.74$, $x_{cub} = 0.39$ (c) $x_{dens} = 0.49$, $x_{or} = 0.48$, $x_{cub} = 0.81$

Fig. 22. Examples of 25×25 cells with the related homogenized stiffness tensor and objective functions obtained by reshaping the 100×100 cells in Figure 12 from the new database (left) and the original EMTO database (right).

Table 4. Comparison of compliances from different methods for the MBB beam problem.

Method	Evaluation grid	Objective function c	vs *top88* 800×600 grid
top88	800×600	65.1	–
Garner's reprojected	800×600	104.2	+37.5%
EMTO			
Homogenized	32×24	58.1	−12.0%
PP - 25×25 cells	800×600	68.4	+4.8%
Ex-EMTO			
Homogenized	32×24	57.2	−13.8%
PP - 25×25 cells	800×600	69.4	+6.2%

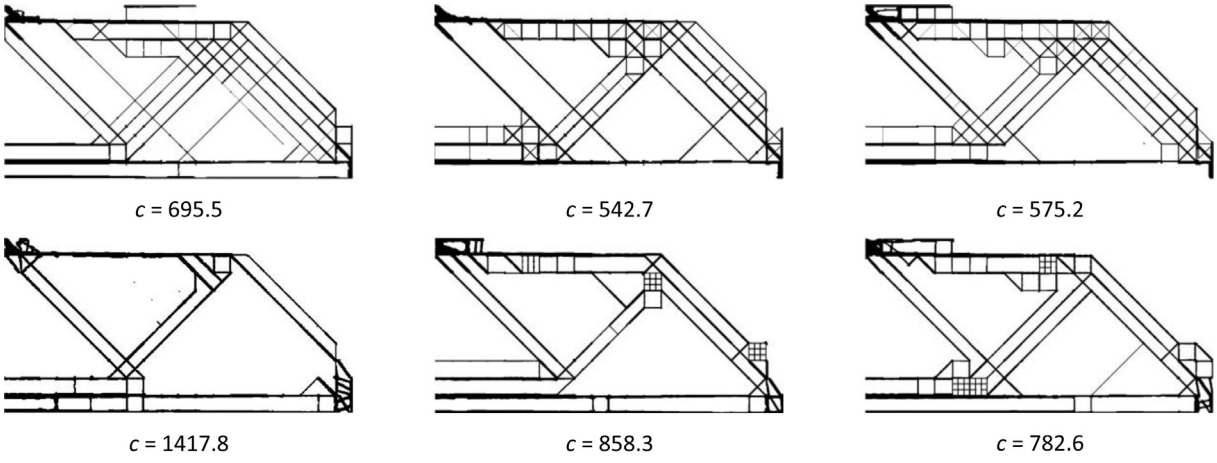

(a) Volume fraction 0.126. (b) Volume fraction 0.127. (c) Volume fraction 0.128.

Fig. 23. Examples obtained for a 20×10 macro-scale grid half MBB beam for different volume fractions, both for the new database (top figures) and the original EMTO one (bottom figures). The compliance is reported below each structure.

5.2 The controlled porosity test case

In Figure 26a the designs obtained by Ex-EMTO and the original EMTO are shown in the case of porosity fixed to 0.5 for a cantilever beam with global volume fraction constraint of 0.5. In Figure 26b the designs in the case of porosity constrained to a minimum value of 0.4 are shown. These two cases are easier to implement imposing limits to the density variable x_{dens}: a same porosity (p_{fixed}) as in equation (6) or a minimum porosity (p_{min}) as in equation (7).

$$x_{dens} = 1 - p_{fixed}, \tag{6}$$

$$x_{dens} \leq 1 - p_{min}, \tag{7}$$

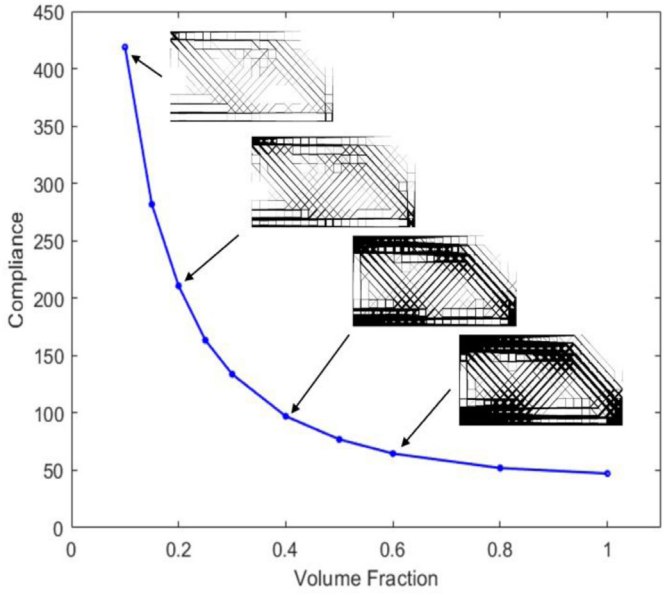

Fig. 24. "Theoretical compliance vs volume fraction" Pareto curve for the 20×10 half MBB beam problem.

In Figure 26 the theoretical compliances or "homogenized" ones (i.e. the compliances computed by using the stiffness tensors form the database) are reported below the designs. The compliances of the Ex-EMTO are a bit higher than the original EMTO ones. This is due to the restrained design space of the unit cells as explained in Section 3.4.

5.3 The fixed topology test case

In Figure 27, the design of Ex-EMTO and original EMTO are shown for a 120×40 cantilever beam in the case of fixed unit cell topology with a global volume fraction constraint of 0.5. The cubicity and the orientation variables are fixed respectively to 0.5 (the principal directions have the same importance) and 0.25 (that stands for an orientation angle of $\boldsymbol{\pi}/4$ *rad*). The designs are really similar and also the values of the theoretical compliances are almost the same. Ex-EMTO seems to give a totally symmetric result. For the optimum, it seems to be slightly better, but it should be remembered that the new database is obtained with a penalization coefficient equals to 1 so a better result for the compliance was expected.

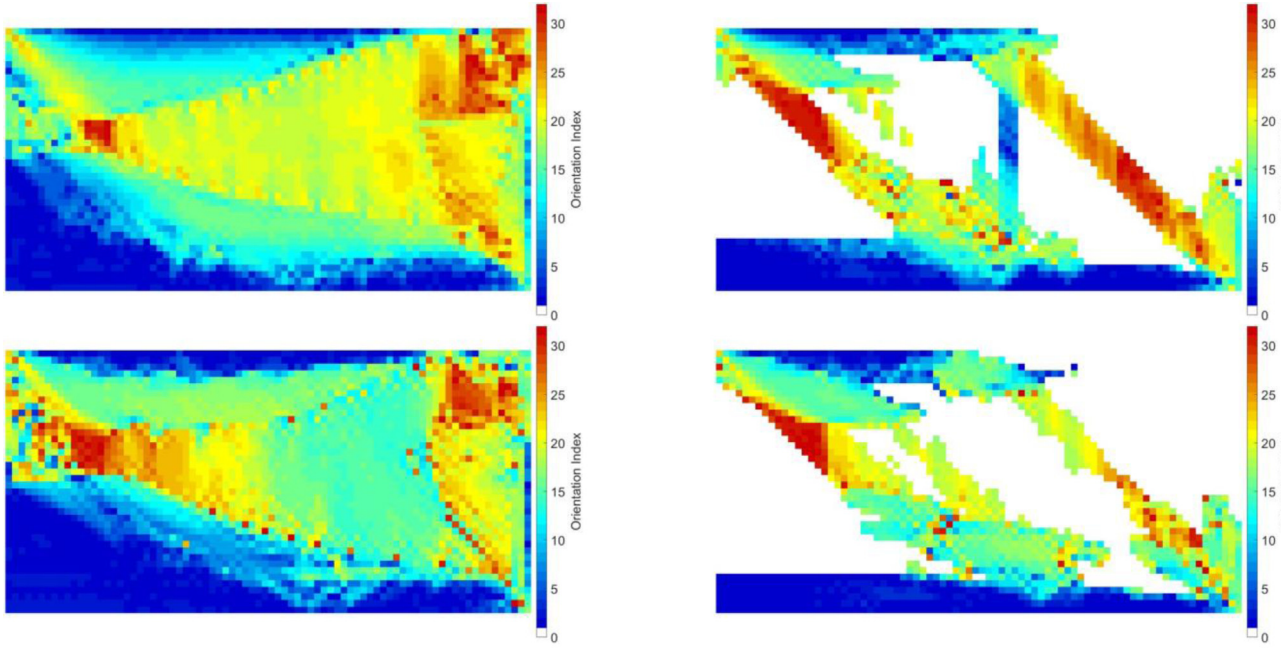

(a) Cells database orientation variable indexes for macro element usage 1 and elements volume fraction 0.5.

(b) Cells database orientation variable indexes for macro element usage 0.5 and elements volume fraction 0.5.

Fig. 25. Examples obtained for a 80×40 half MBB beam for the new database (top figures) and the original one (bottom figures).

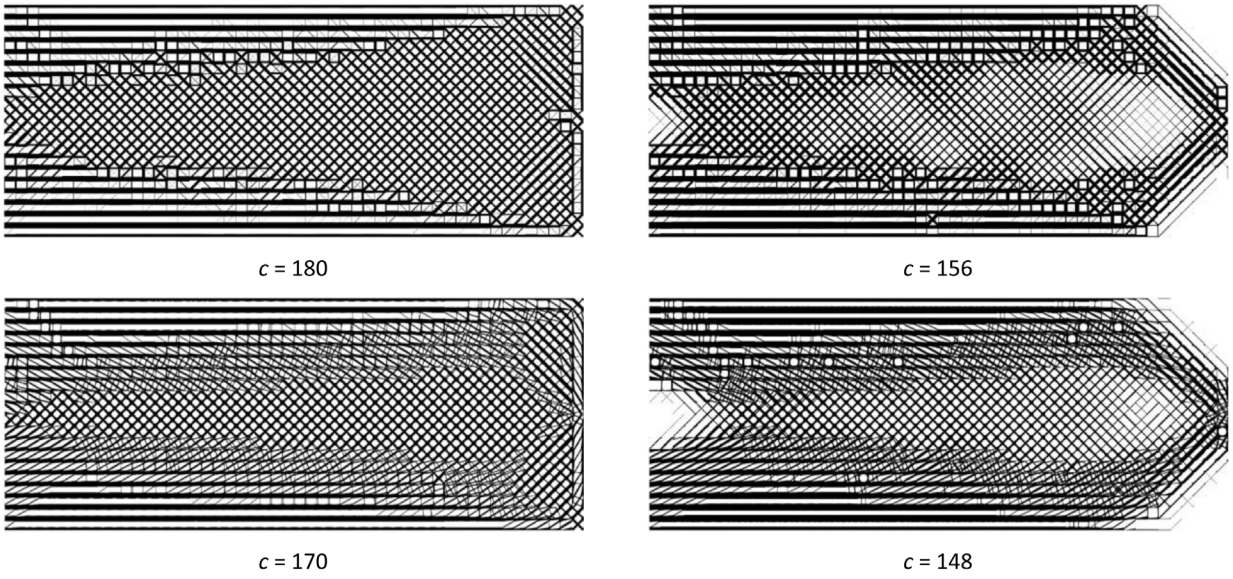

(a) Design obtained for a cantilever beam when the porosity is fixed to 0.5 for every micro-structure.

(b) Design obtained for a cantilever beam where a minimum porosity of 0.4 is applied.

Fig. 26. Examples obtained for a 50×20 cantilever beam with restrained porosity both for the new database (top figures) and the original EMTO one (bottom figures).

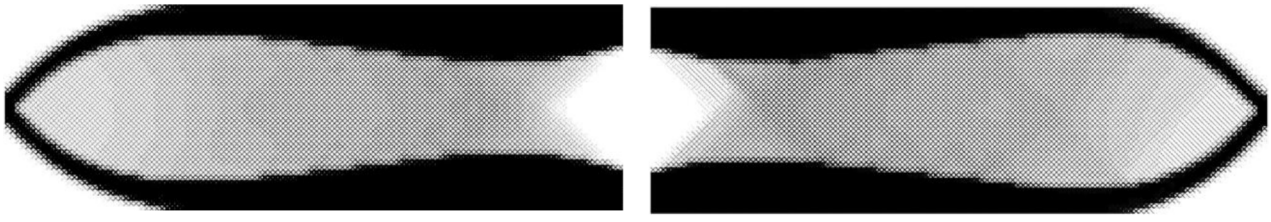

(a) Design obtained by varying only the density with the new database. The theoretical compliance is equal to 186.

(b) Design obtained by varying only the density with the original database. The theoretical compliance is equal to 188.

Fig. 27. Example obtained for a 120×40 cantilever beam by limiting the design space.

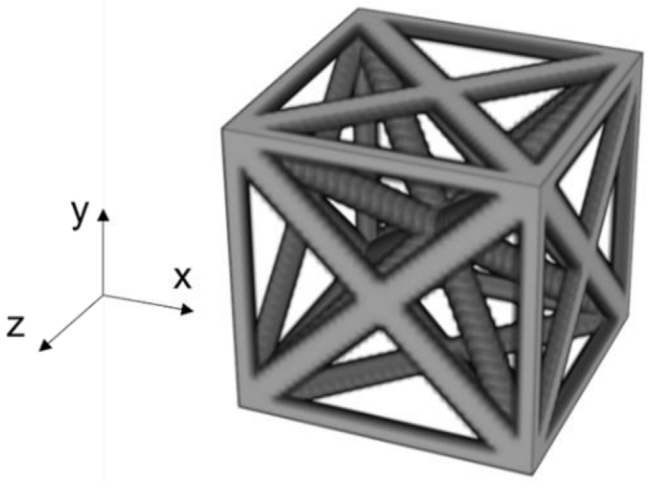

Fig. 28. 3D unit cell obtained by superimposing beams.

6 Conclusions

In this paper a different approach to build the unit cell for the EMTO is developed. Here we restricted ourselves to the two-dimensional case, postponing its application to the three-dimensional cases for other communications. In the 2D case, the connectivity is assured by considering intrinsically well-connected unit cells instead of using the transmission zones. Despite the reduction of the design space of the micro-structures, the efficiency and versatility of the EMTO method is demonstrated thanks to the results of the parametrized cells similar to the ones of the free cells. Moreover, the new developed approach to construct the unit cells leads to some advantages:

– A lighter database, since it is not necessary to store all the 100×100 elements of the optimal micro-structure, but just the 4 parameters;

– The possibility to introduce more easily additive manufacturing constraints, since minimum and maximum thicknesses for the beams can be defined both in the unit cell code and in the micro-optimization;
– The resulting macro-structures are surely made of beams, without the risk to have very strange shapes;
– The possibility to reshape more easily the micro-structures reducing the computational cost of the full-scale evaluation.

Future works include speeding up the codes, adding additive manufacturing constraints and validate the results by testing printed structures obtained by the method. Lately, it is also worth mentioning that the foregoing two-dimensional analysis is currently being extended to three-dimensional case. The 3D case has to deal with a higher number of parameters to build the 3D unit cell shown in Figure 28, as well as higher computational effort and complexity. It will be presented in a forthcoming communication.

Appendix A: Surrogate prediction

The Nadaraya–Watson's kernel-weighted average with a Gaussian Kernel G

$$\boldsymbol{E}_{pred}(x^i) = \frac{\sum_{l=1}^{k} G(x^i, x_l)\boldsymbol{E}_{db}(x_l)}{\sum_{l=1}^{k} G(x^i, x_l)},$$

$$G(x^i, x_l) = exp\left(- \frac{d_{eucl}(x^i, x_l)^2}{2b^2} \right).$$

Here $\boldsymbol{E}_{pred}(x^i)$ is the predicted stiffness tensor of the cell corresponding to the set of macro-design variable $x^i = [x^i_{dens}, x^i_{or}, x^i_{cub}]$ x_l are the points in the database and $\boldsymbol{E}_{db}$ (x_l) are the database stiffness tensors of the cells corresponding to those points; b is the kernel radius; d_{eucl} $(x^i,\ x_l)$ measures the Euclidean distance between x^i and x_l.

Appendix B: top88 results

Fig. B1. Comparison of half MBB designs. a top88 design on a 32×24 grid and b top88 design on a 800×600 grid.

Acknowledgements

The authors are grateful to the anonymous reviewers for their expertise, their very helpful and referenced comments, proofreading and checking.

Funding

The authors would like to thank Erasmus + Programme for funding this research.

Conflict of interest

The authors declare that they have no conflict of interest.

Data availability

The codes and the unit-cell databases are available on GitHub for reproducible research purpose (https://github.com/mid2SUPAERO/Ex-EMTO) [40].

Author contribution statement

Each named author has substantially contributed to conducting the underlying research and drafting this manuscript.

References

[1] W. Prager, G. Rozvany, Optimization of structural geometry, in: A. Bednarek, L. Cesari (Eds.), Dynamical Systems. Academic Press, 1977, pp. 265–293
[2] M.P. Bendsøe, N. Kikuchi, Generating optimal topologies in structural design using a homogenization method, Appl. Mech. Eng. **71**, 197–224 (1988)
[3] M.P. Bendsøe, Optimal shape design as a material distribution problem, Struct. Optim. **1**, 193–202 (1989)
[4] O. Sigmund, Materials with prescribed constitutive parameters: an inverse homogenization problem, Int. J. Solids Struct. **31**, 2313–2329 (1994)
[5] Y. Xie, G. Steven, A simple evolutionary procedure for structural optimization, Comput. Struct. **49**, 885–896 (1993)
[6] G. Allaire, F. Jouve, A.-M. Toader, A level-set method for shape optimization, C.R. Acad. Sci. Paris, Série I, **334**, 1125–1130 (2002)
[7] M. Zhou, G. Rozvany, The coc algorithm, part ii: Topological, geometrical and generalized shape optimization, Comput. Methods Applied Mech. Eng. **89**, 309–336 (1991)
[8] M.P. Bendsøe, O. Sigmund, Material interpolation schemes in topology optimization, Archive of Applied Mechanics **69**, 635–654 (1999)
[9] V. Challis, A. Roberts, A. Wilkins, Design of three dimensional isotropic microstructures for maximized stiffness and conductivity, Int. J. Solids Struct. **45**, 4130–4146 (2008)
[10] X. Huang, A. Radman, Y. Xie, Topological design of microstructures of cellular materials for maximum bulk or shear modulus, Comput. Mater. Sci. **50**, 1861–1870 (2011)
[11] Y.M. Xie, X. Yang, J. Shen, X. Yan, A. Ghaedizadeh, J. Rong, X. Huang, S. Zhou, Designing orthotropic materials for negative or zero compressibility, Int. J. Solids Struct. **51**, 4038–4051 (2014)
[12] O. Sigmund, S. Torquato, Design of materials with extreme thermal expansion using a three-phase topology optimization method, J. Mech. Phys. Solids **45**, 1037–1067 (1997)
[13] J. Wu, O. Sigmund, J.P. Groen, Topology optimization of multi-scale structures: a review, Struct. Multidiscipl. Optim. **63**, 1455–1480 (2021)

[14] Y. Wang, H. Xu, D. Pasini, Multiscale isogeometric topology optimization for lattice materials, Comput. Methods Appl. Mech. Eng. **316**, 568–585 (2017)
[15] S. Watts, W. Arrighi, J. Kudo, D. Tortorelli, D. White, Simple, accurate surrogate models of the elastic response of three-dimensional open truss micro-architectures with applications to multiscale topology design, Struct. Multidiscipl. Optim. **60**, 1887–1920 (2019)
[16] S. Zhou, Q. Li, Microstructural design of connective base cells for functionally graded materials, Mater. Lett. **62**, 4022–4024 (2008)
[17] E. Garner, H.M. Kolken, C.C. Wang, A.A. Zadpoor, J. Wu, Compatibility in microstructural optimization for additive manufacturing, Addit. Manuf. **26**, 65–75 (2019)
[18] L. Xia, P. Breitkopf, Concurrent topology optimization design of material and structure within fe2 nonlinear multiscale analysis framework, Comput. Methods Appl. Mech. Eng. **278**, 524–542 (2014)
[19] L. Xia, P. Breitkopf, Multiscale structural topology optimization with an approximate constitutive model for local material microstructure, Comput. Methods Appl. Mech. Eng. **286**, 147–167 (2015b)
[20] C. Wang, J. Zhu, W. Zhang, S. Li, J. Kong, Concurrent topology optimization design of structures and non-uniform parameterized lattice microstructures, Struct. Multidiscipl. Optim. **58**, 35–50 (2018)
[21] C. Imediegwu, R. Murphy, R. Hewson, M. Santer, Multiscale structural optimization towards three-dimensional printable structures, Struct. Multidiscipl. Optim. **60**, 513–525 (2019)
[22] C. Wang, X. Gu, J. Zhu, H. Zhou, S. Li, W. Zhang, Concurrent design of hierarchical structures with three-dimensional parameterized lattice microstructures for additive manufacturing, Struct. Multidiscipl. Optim. **61**, 869–894 (2020)
[23] N. Ferro, S. Perotto, D. Bianchi, R. Ferrante, M. Mannisi, Design of cellular materials for multiscale topology optimization: application to patient-specific orthopedic devices, Struct. Multidiscipl. Optim. **65**, 79 (2022)
[24] O. Pantz, K. Trabelsi, A post-treatment of the homogenization method for shape optimization, SIAM J. Control Optim. **47**, 1380–1398 (2008)
[25] G. Allaire, P. Geoffroy-Donders, O. Pantz, Topology optimization of modulated and oriented periodic microstruc-tures by the homogenization method, Comput. Math. Appl. **78**, 2197–2229 (2019)
[26] P. Geoffroy-Donders, G. Allaire, O. Pantz, 3-d topology optimization of modulated and oriented periodic micro-structures by the homogenization method, J. Comput. Phys. 108994 (2019)
[27] J.P. Groen, O. Sigmund, Homogenization-based topology optimization for high-resolution manufacturable mi-crostructures, Int. J. Numer. Methods Eng. **113**, 1148–1163 (2018)
[28] E. Duriez, J. Morlier, M. Charlotte, C. Azzaro-Pantel, A well connected, locally-oriented and efficient multi-scale to-pology optimization (emto) strategy, Struct. Multidiscipl. Optim. **64**, 3705–3728 (2021)
[29] L. Xia, P. Breitkopf, Design of materials using topology optimization and energy-based homogenization approach in matlab, Struct. Multidiscipl. Optim. **52**, 1229–1241 (2015a)
[30] Z. Xia, Y. Zhang, F. Ellyin, A unified periodical boundary conditions for representative volume elements of compo-sites and applications, Int. J. Solids Struct. **40**, 1907–1921 (2003)
[31] Z. Wu, L. Xia, S. Wang, T. Shi, Topology optimization of hierarchical lattice structures with substructuring, Comput. Methods Appl. Mech. Eng. **345**, 602–617 (2019)
[32] C. Zhang, S. Xu, J. Liu, Y. Ma, Comprehensive clustering-based topology optimization for connectable multi-scale additive manufacturing structures, Addit. Manuf. **54**, 102786 (2022)
[33] E. Andreassen, A. Clausen, M. Schevenels, B.S. Lazarov, O. Sigmund, Efficient topology optimization in matlab us-ing 88 lines of code, Struct. Multidiscipl. Optim. **43**, 1–16 (2011)
[34] O. Sigmund, A 99 line topology optimization code written in matlab, Struct. Multidiscipl. Optim. **21**, 120–127 (2001)
[35] E.A. Nadaraya, On estimating regression, Theory Probab. Appl. **9**, 141–142 (1964)
[36] K. Svanberg, The method of moving asymptotes — a new method for structural optimization, Int. J. Numer. Methods Eng. **24**, 359–373 (1987)
[37] J. Wallach, L. Gibson, Mechanical behavior of a three-dimensional truss material, Int. J. Solids Struct. **38**, 7181–7196 (2001)
[38] L. Liu, J. Yan, G. Cheng, Optimum structure with homogeneous optimum truss-like material, Comput. Struct. **86**, 1417–1425 (2008)
[39] M.P. Schmidt, C.B.W. Pedersen, C. Gout, On structural topology optimization using graded porosity control, Struct. Multidiscipl. Optim. **60**, 1437–1453 (2019)
[40] Open-source available on GitHub for reproducible research purpose (https://github.com/mid2SUPAERO/Ex-EMTO)

Cite this article as: A. Di Rienzo, E. Duriez, M. Charlotte, J. Morlier, Lightweighting structures using an explicit microarchitectured material framework, Mechanics & Industry **25**, 7 (2024)